

Highly sensitive layered ZnO/LiNbO₃ SAW device with InO_x selective layer for NO₂ and H₂ gas sensing

S.J. Ippolito^{a,b,*}, S. Kandasamy^a, K. Kalantar-zadeh^{a,b}, W. Wlodarski^{a,b},
K. Galatsis^c, G. Kiriakidis^d, N. Katsarakis^d, M. Suchea^d

^a School of Electrical and Computer Engineering, RMIT University, Melbourne, Australia

^b CRC for MicroTechnology, Australia

^c Functional Engineered Nano Architectonics, University of California, Los Angeles, CA, USA

^d Institute of Electronic Structure and Laser, Foundation for Research and Technology-Hellas, Greece

Available online 26 August 2005

Abstract

Layered surface acoustic wave (SAW) devices for the monitoring of NO₂ and H₂ in synthetic air have been fabricated on XZ LiNbO₃ with a 1.2 μm ZnO guiding layer. To increase selectivity and sensitivity, InO_x layers of thickness 40 and 200 nm were employed. The sensor's performance was analyzed in terms of frequency shift as a function of different gas concentrations. The sensors were tested over a range of operating temperatures between 100 and 273 °C. A large response magnitude with fast response and recovery time was observed. Positive frequency shifts of 91 kHz for 2.125 ppm of NO₂ and negative frequency shifts of 319 kHz for 1% of H₂ in synthetic air are presented; demonstrating the high sensitivity of the layered SAW structure with the DC sputtered InO_x thin film. The surface of the layered SAW structure was studied by atomic force microscopy (AFM) before and after the deposition of the InO_x selective layer. The AFM analysis demonstrates that the InO_x films deposited on ZnO, the guiding layer, resulted in an increase in surface area due to the highly uniform nanostructured surface morphology of InO_x.

© 2005 Elsevier B.V. All rights reserved.

Keywords: Layered; SAW; Indium oxide; InO_x; Nitrogen dioxide; Hydrogen

1. Introduction

The change in electrical resistance caused by the adsorption of a target gas on the surface of a semiconductor has been well documented [1]. Metal oxides such as SnO₂, WO₃ and TiO₂ are well known for their high sensitivity to changes in the different gas atmospheres. Indium oxide has shown to be sensitive towards both oxidizing and reducing gases, making it a promising material for gas sensing applications. Takada et al. first reported resistive type ozone sensors based on InO_x thin films [2,3]. The sensing mechanism is based on the adsorption of ozone molecules on the surface of the sensing film, which increases the film resistance [4].

The detection of oxidizing gases such as Cl₂ and NO₂ in the ppb and ppm ranges has been reported [5,6]. Gurlo et al.

have shown that nanocrystalline In₂O₃ thin films, prepared by sol–gel method, showed high sensitivity towards NO₂ [7]. Other studies have shown sensitivity towards NO₂ that increases with a decrease in In₂O₃ grain size [8]. Furthermore, data regarding detection of reducing gases such as CO and H₂ has been reported in Refs. [9,10]. Increased selectivity towards CO was later demonstrated by Yamaura et al., with the addition of cobalt oxide or gold to the In₂O₃ layer [11].

Indium oxide and indium tin oxide films are known to exhibit a change in band-gap depending upon the oxygen concentration in the film [12,13]. Indium oxide in its stoichiometric form (In₂O₃), behaves as an insulator. Whereas, in its non-stoichiometric form (InO_x), it can behave as an n-type semiconductor as a result of intrinsic defects and oxygen vacancies [14]. The oxygen vacancies in the InO_x film act as donors and the sample's conductivity can be changed by controlling the oxygen deficiencies [15].

* Corresponding author.

E-mail address: sipp@ieee.org (S.J. Ippolito).

InO_x is a material of fundamental interest because the film's conductivity can be altered drastically by post-growth annealing, UV radiation or exposure to ozone [14]. Different fabrication techniques and treatments have shown to produce numerous indium oxide varieties with different electrical and optical properties. The conductivity of amorphous InO_x films has been shown to change reversibly by exposing the films to UV light (under vacuum) or to an oxidizing ambient. However, crystallized InO_x was not shown to exhibit the photoreduction and oxidation processes observed in the amorphous InO_x [15].

Previous work regarding the InO_x films showed sensitive and repeatable gas sensing characteristics towards both O_3 and NO_2 at operating temperatures between 50 and 300 °C [16]. For results presented here, two different thickness of InO_x , 40 and 200 nm, respectively, have been deposited on the surface of $\text{ZnO}/\text{LiNbO}_3$ layered surface acoustic wave (SAW) devices. The devices are investigated for their NO_2 and H_2 gas sensing properties at different operating temperatures. It is widely known that SAW devices show high sensitivity towards electrical perturbations and have been studied for sensing applications since 1979 [17]. The interactions of NO_2 and H_2 gases with the InO_x thin film cause its conductivity to change, resulting in a predictable effect on the propagating acoustic wave. By using a layered SAW device, it is possible to enhance the structure's sensitivity to such interactions. This is achieved by deposition of the selective layer over the entire surface of the structure. Furthermore, the layer allows to match the sheet conductivity of the substrate to the selective layer [18], further increasing the overall sensitivity.

Results presented here show the device's performance, analyzed in terms of frequency shift (response magnitude) as a function of operational temperature and different NO_2 and H_2 gas concentrations. Extremely strong frequency shifts of positive 91 kHz for 2.125 ppm of NO_2 and negative frequency shifts of 319 kHz for 1% of H_2 in synthetic air were observed. Furthermore, characterization of the ZnO guiding layer and InO_x selective thin film by atomic force microscopy (AFM) are presented.

2. Layered SAW device fabrication

The layered SAW devices were fabricated on XZ LiNbO_3 wafers. Metal layers of Al (2500 Å) and Cr adhesion layer (300 Å) were deposited by electron beam evaporation. A periodicity of 24 μm for the IDTs was patterned using a wet-etch process to create a two-port delay line with 64 finger pairs in each port. The center-to-center distance and aperture width for the IDT structure was 85 wavelengths (λ) and 1.25 mm, respectively.

A 1.2 μm piezoelectric guiding layer of ZnO was deposited over the patterned IDTs using RF magnetron sputtering. A sputtering pressure of 1.3×10^{-2} mbar was achieved using 40% oxygen balanced in argon. The sputtering

process was conducted for 60 min at a substrate temperature of 260 °C. A 99.99% pure ZnO target was utilized. An RF power of 120 W resulted in a deposition rate of 20 nm/min.

Finally, an InO_x thin film was deposited over the ZnO guiding layer using DC sputtering to form the selective layer. A 40 nm InO_x thin film was deposited on the first layered SAW device. Similarly, a 200 nm thick InO_x layer was deposited on the second device. A 99.999% pure metallic indium target and 100% oxygen plasma, at 1.5×10^{-2} mbar were used. The deposition temperature was maintained between 24 and 40 °C with a current and voltage of 0.15 A and 300 V, respectively. Ex situ thickness measurements confirmed a deposition rate of approximately 3 nm/min.

2.1. Surface characterization

AFM characterization of the surface of the layered SAW structure was made before and after the deposition of the InO_x selective layer. The surface morphology (grain sizes and surface roughness) was investigated with a Nanoscope III atomic force microscope in tapping mode. Roughnesses (RMS) of 27.03 and 10.12 nm were measured after the deposition of the InO_x on the metallised and non-metallised regions of the structure, respectively. Measurements were conducted over a $5 \mu\text{m} \times 5 \mu\text{m}$ area. Fig. 1 illustrates the detail, $50 \mu\text{m} \times 50 \mu\text{m}$ on the fingers region of the SAW device. A mean grain radius of 70 nm was measured in the area corresponding to the non-metallised region of the structure. The difference in growth between the metallised and non-metallised regions is due to the substrate's strong influence in the initial growth of the 1.2 μm thick ZnO guiding layer. The rough metallic surface behavior is reflected in an RMS of 21.58 nm for ZnO on metal and an RMS of 7.37 nm for the ZnO on the smoother interfinger-corresponding substrate.

Fig. 2 shows the AFM image of the same 40 nm InO_x film deposited on silicon substrate (orientation, 100). An image area of $1 \mu\text{m} \times 1 \mu\text{m}$ is shown with a z -range of 5 nm within a z -scale of 7 nm. A significantly smaller roughness of

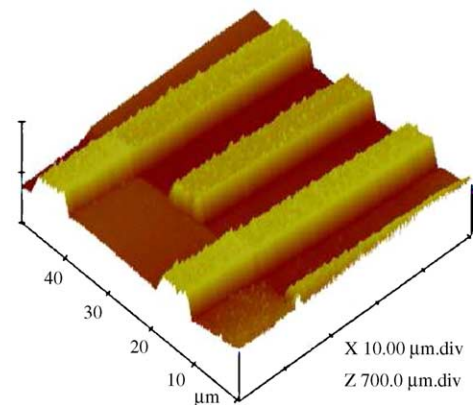


Fig. 1. AFM image of a detail $50 \mu\text{m} \times 50 \mu\text{m}$ on the fingers region of the SAW device.

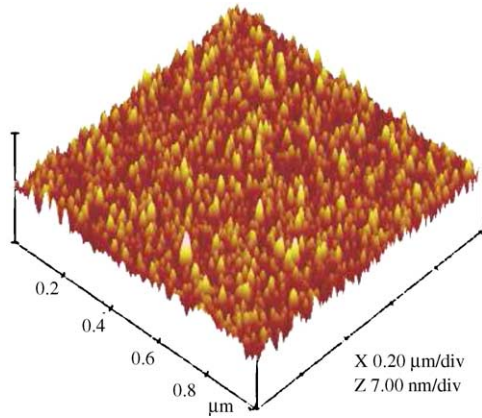


Fig. 2. AFM surface image of 40 nm InO_x layer deposited on silicon substrate. A surface roughness of 0.61 nm with a grain radius of 19 nm was measured.

0.610 nm was measured in the same conditions as the above values ($5 \mu\text{m} \times 5 \mu\text{m}$ scan size area). A mean grain radius of 19 nm was calculated over a high-resolution $1 \mu\text{m} \times 1 \mu\text{m}$ scan size area.

Further AFM characterization regarding the deposition of InO_x thin films on silicon and corning glass substrates can be

found elsewhere [19,20]. The different growth behavior of InO_x on the layered SAW structure and the silicon substrate can be directly attributed to the surface roughness differences of the ZnO grown on the XZ LiNbO_3 and metallic substrates as discussed before.

Figs. 3 and 4 show the surface of the structure before and after deposition of the InO_x layer on the non-metallised regions of the layered SAW structure, $1 \mu\text{m} \times 1 \mu\text{m}$ areas with the z-range between 50 and 75 nm are presented. It can be seen that the surface, after InO_x deposition on the structure, exhibits features with facets comparable with the rather rough structure of the ZnO layer prior to the InO_x deposition. This is also the case where the ZnO grains grow substantially different on the metallised regions, suggesting that the 40 nm thin InO_x film follows the initial ZnO surface topology.

After deposition, the image z-range increases and the shape of the grains become well defined. This is particularly visible in the top view images, suggesting an improvement in surface crystallinity. The measured roughness of 7.37 nm before InO_x deposition, increased to 10.12 nm after deposition; an increase of approximately 37%. At the same time, the size of the surface features (in the z-range) showed an increase of approximately 25%, from roughly 50 nm features for the ZnO substrate before InO_x deposition to 75 nm afterwards.

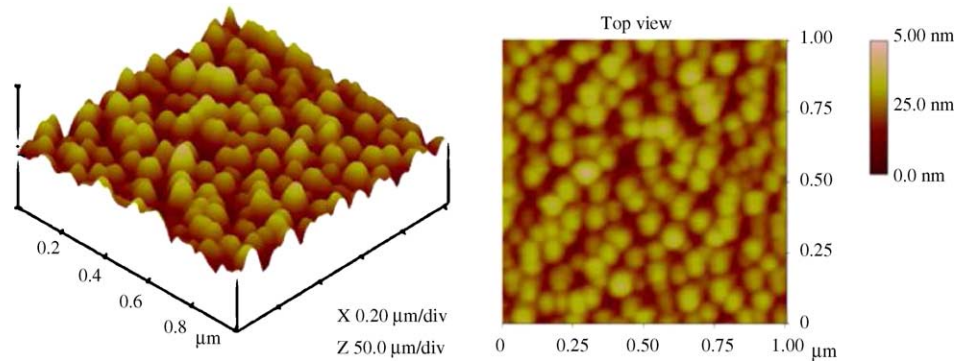


Fig. 3. AFM surface image of 1.2 μm thick ZnO deposited on non-metallised XZ LiNbO_3 substrate. A surface roughness of 7.37 nm with 50 nm surface features (in the z-scale) is illustrated.

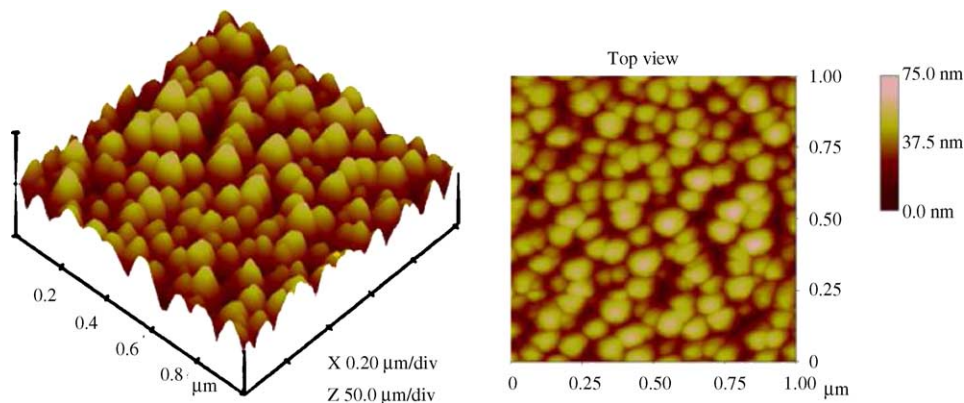


Fig. 4. AFM surface image of 40 nm InO_x layer deposited on top of the 1.2 μm thick ZnO on non-metallised XZ LiNbO_3 substrate. Analysis shows an increased surface feature size of 75 nm (in the z-scale) and a roughness of 10.12 nm.

3. Gas sensing results

The SAW devices were mounted on a micro-heater and enclosed in a teflon based gas chamber, approximately 30 ml in volume. The micro-heater was controlled by a regulated DC power supply, which provided different operating temperatures. Using a computerized multi-channel gas calibration system, each device was exposed to a sequence of NO₂, H₂ and CO gas pulses over a range of operating temperatures between 100 and 273 °C. The exposed NO₂ and H₂ gas concentration range was from 510 ppb to 8.5 ppm and from 0.06 to 1.0% in synthetic air, respectively. The synthetic air composed of 20% oxygen balanced in nitrogen. Exposure to CO concentrations was between 60 and 1000 ppm in synthetic air. A constant flow rate of 0.200 l/min and certified gas bottles balanced in synthetic air were used. At each operating temperature, the baseline gas was maintained for a period of 90 min to allow the device to stabilize. Then, the device was exposed to the different concentration sequences of NO₂, H₂ and CO for several hours.

Both 40 and 200 nm InO_x layer SAW devices were tested separately. However, the devices were tested under the same conditions using the same sequence of gas exposure. The SAW devices were used as a positive feedback element in a closed-loop circuit, along with an amplifier, to form an oscillator. Thus, the frequency of the system could then be correlated to the corresponding target gas concentration. The operating frequencies for the 40 and 200 nm devices at room temperature were 138.2 and 139.6 MHz, respectively. A computer was used to data-log a frequency counter (Fluke PM6680B) that monitored the oscillation frequency.

3.1. Response to NO₂

The NO₂ absorption and desorption on the InO_x selective layer causes velocity perturbations in the acoustic waves travelling at the surface of the device. The NO₂ reduces the InO_x layer's conductivity, resulting in an increase in the acoustic wave velocity. This, therefore, results in the oscillation frequency increasing in the presence of NO₂.

Each NO₂ gas sequence consisted of 510 ppb, 1.063 ppm, 2.125 ppm, 4.2 ppm and 8.5 ppm balanced in synthetic air. A second pulse of 1.063 ppm was used to confirm its repeatability. The exposure and recovery time used were fixed at 180 and 360 s, respectively. Fig. 5 shows the dynamic response to the NO₂ sequence at an operating temperature of 246 °C for both the 40 and 200 nm devices. A frequency shift in excess of 91 and 18 kHz was observed for the 40 and 200 nm devices towards 4.25 ppm of NO₂, respectively. The saturation concentration for both devices was found to be approximately 2.125 ppm of NO₂. Increasing the NO₂ concentration above this level did not result in a significant increase in frequency shift.

Fig. 6 shows the temperature dependence on the frequency shift for 510 ppb and 2.125 ppm NO₂ concentrations. It can be seen that the 40 nm InO_x device outperforms the 200 nm

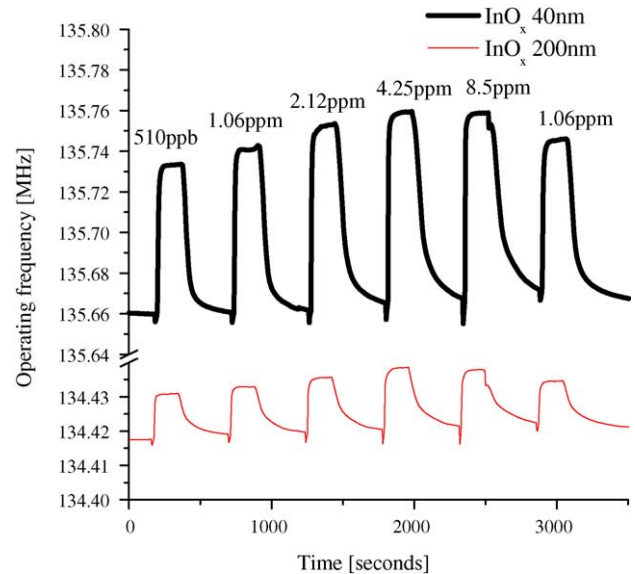


Fig. 5. Response of 40 nm (top) and 200 nm (bottom) InO_x layered SAW devices towards a sequence of NO₂ pulses at 246 °C.

device. The highest frequency shift was obtained at 246 and 218 °C for the 40 and 200 nm, respectively. Although the 200 nm device produced its highest frequency shift at 218 °C, frequency shifts for all NO₂ concentrations test were observed to be approximately the same magnitude. Therefore, the 200 nm device could only be used at an operating temperature of 246 °C before a meaningful correlation between frequency shift and NO₂ gas concentration could be established.

3.2. Response to H₂

Unlike NO₂, H₂ increases the conductivity of the InO_x selective layer by injecting electrons into the surface. This

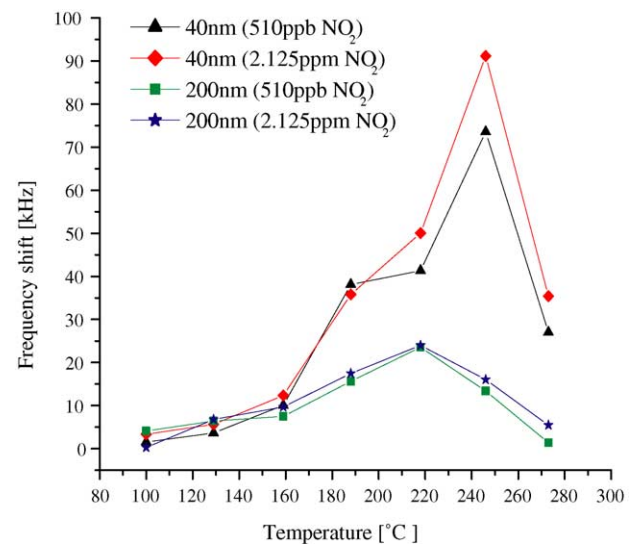


Fig. 6. Frequency shift vs. operating temperature for 40 and 200 nm InO_x layered SAW devices towards NO₂.

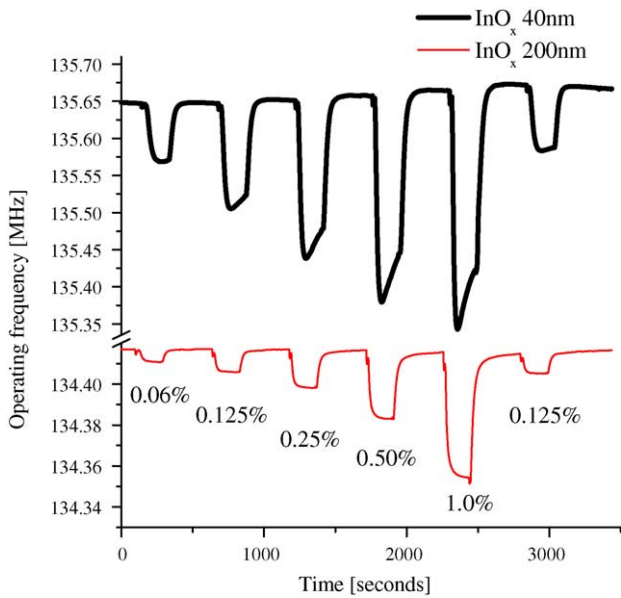


Fig. 7. Response of 40 nm (top) and 200 nm (bottom) InO_x layered SAW devices towards a sequence of H₂ pulses at 246 °C.

results in a decrease in the acoustic wave velocity, thereby a decrease in the oscillation frequency is observed in the presence of H₂ gas.

The H₂ pulse sequence consisted of 0.06, 0.125, 0.25, 0.5, 1.0 and 0.125% in synthetic air and was tested over each operating temperature. The dynamic response of the 40 and 200 nm InO_x devices to the H₂ sequence is shown in Fig. 7 at an operating temperature of 246 °C. The 200 nm layer did not exhibit an overshoot in response which is clearly present in the 40 nm layer. At operating temperatures at and below 218 °C, the overshoot present in the 40 nm device subsided.

Responses towards H₂ gas concentrations of 0.06–1.0% were in the order of 78.5–319.4 kHz for the 40 nm layer and

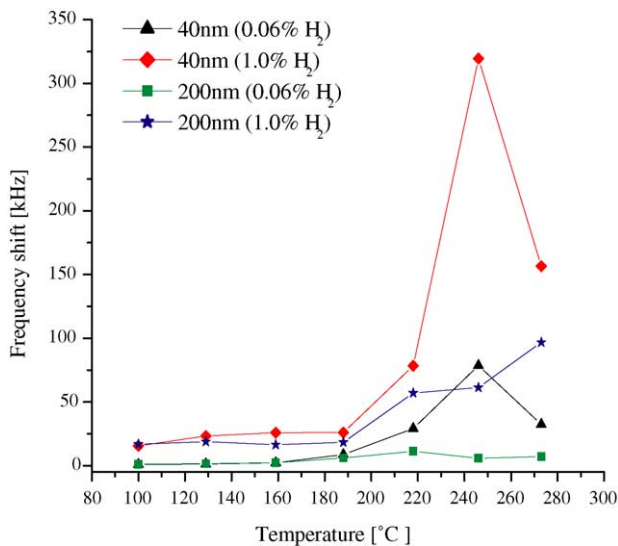


Fig. 8. Frequency shift vs. operating temperature for 40 and 200 nm InO_x layered SAW devices towards H₂.

5.7–61.3 kHz for the 200 nm layer, respectively. The response of both devices did not appear to saturate, showing a large dynamic range. Fig. 8 shows the frequency shift observed at each tested operating temperature for 0.06 and 1% H₂ concentrations. Maximum frequency shift was observed at 246 °C for the 40 nm device. However, an increasing trend in frequency shift is apparent for the 200 nm device for temperatures over 273 °C. Limitations in the experimental setup prevented testing above this temperature.

4. Discussion and conclusions

From results presented, it can be seen that the 40 nm InO_x layer largely outperforms the 200 nm, for both NO₂ and H₂ gases. Fig. 9 illustrates a comparison between both devices at an operating temperature of 246 °C. The large difference in frequency shift for both the 40 and 200 nm devices is shown. Furthermore, the saturation of NO₂ at 2.125 ppm is apparent.

Due to the InO_x deposited on the ZnO surface possessing a different surface morphology than the InO_x on silicon or glass substrate, a correlation between the sensing properties with grain size distribution and surface morphology is required. Based on previous measurements for InO_x deposited on silicon and corning glass substrates [21], it is shown that the film thickness has strong influence on the film surface morphology, and the surface morphology plays an essential role on gas sensing properties of the films. This can explain the differences in sensitivity between 40 and 200 nm InO_x layers. Attempts to explain the interaction mechanism of NO₂, H₂, O₃ and CO with In₂O₃ have been presented in the literature [9,22]. However, a lack of knowledge exists concerning the interaction mechanism with the oxygen deficient InO_x layers for gas sensing applications.

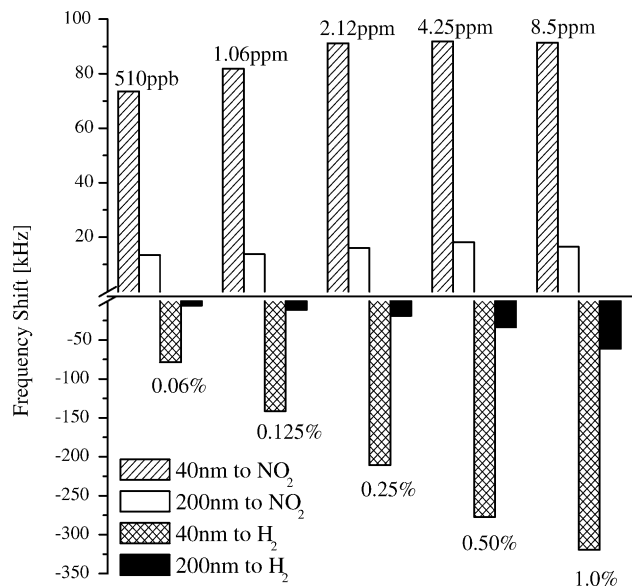


Fig. 9. Frequency shift vs. concentration of NO₂ and H₂ gases for 40 and 200 nm InO_x layered SAW devices at 246 °C.

Unusually, both the 40 and 200 nm layers did not show any significant response towards CO concentrations as high as 1000 ppm at all tested operating temperatures. This is contrary to findings by Korotcenkov et al. [9] and Yamaura et al. [10,11] leading the authors to believe that the deposited InO_x film used do not possess a high affinity towards CO when compared to In_2O_3 thin films. This could also be compounded by the effect of the ZnO layer influencing the morphology of the InO_x thin film.

Consequently, the layered SAW structure in conjunction with the InO_x film was found to be highly sensitive towards low concentrations of NO_2 and medium concentrations of H_2 gas. Exceptionally strong frequency shifts of positive 91 kHz for 2.125 ppm of NO_2 and negative 319 kHz for 1% H_2 in synthetic air were observed for the 40 nm InO_x layer. Due to the high sensitivity of the 40 nm InO_x layer on the 1.2 μm ZnO/XZ LiNbO_3 SAW structure, it would be an excellent candidate sub-ppm NO_2 gas sensing.

Acknowledgements

The authors would like to thank the CRC for MicroTechnology, Australia, and EU projects HPRN-CT-2002-00298 and ENK6-CT-2002-00678 for funding and financial support.

References

- [1] K. Zakrzewska, Mixed oxides as gas sensors, *Thin Solid Films* 391 (2001) 229–238.
- [2] T. Takada, Ozone detection by In_2O_3 thin film gas sensor, in: T. Seiyama (Ed.), *Chemical Sensor Technology*, Elsevier, Amsterdam, 1988, pp. 59–70.
- [3] T. Takada, K. Suzuki, M. Nakane, Highly sensitive ozone sensor, *Sens. Actuators, B* 13–14 (1993) 404–407.
- [4] M.Z. Atashbar, B. Gong, H.T. Sun, W. Wlodarski, R. Lamb, Investigation on ozone-sensitive In_2O_3 thin films, *Thin Solid Films* 354 (1999) 222–226.
- [5] A. Gurlo, N. Bârsan, M. Ivanovskaya, U. Weimar, W. Göpel, In_2O_3 and $\text{MoO}_3\text{-In}_2\text{O}_3$ thin film semiconductor sensors: interaction with NO_2 and O_3 , *Sens. Actuators, B* 47 (1998) 92–99.
- [6] H. Steffes, C. Imawan, F. Solzbacher, E. Obermeier, Fabrication parameters and NO_2 sensitivity of reactively RF-sputtered In_2O_3 thin films, *Sens. Actuators, B* 68 (2000) 249–253.
- [7] A. Gurlo, M. Ivanovskaya, A. Pfau, U. Weimar, W. Göpel, Sol-gel prepared In_2O_3 thin films, *Thin Solid Films* 307 (1997) 288–293.
- [8] A. Gurlo, M. Ivanovskaya, N. Bârsan, M. Schweizer-Berberich, U. Weimar, W. Göpel, A. Diéguez, Grain size control in nanocrystalline In_2O_3 semiconductor gas sensors, *Sens. Actuators, B* 44 (1997) 327–333.
- [9] G. Korotcenkov, V. Brinzari, A. Cerneavski, M. Ivanov, A. Cornet, J. Morante, A. Cabot, J. Arbiol, In_2O_3 films deposited by spray pyrolysis: gas response to reducing (CO , H_2) gases, *Sens. Actuators, B* 98 (2004) 122–129.
- [10] H. Yamaura, T. Jinkawa, J. Tamaki, K. Moriya, N. Miura, N. Yamazoe, Indium oxide-based gas sensor for selective detection of CO, *Sens. Actuators, B* 35–36 (1996) 325–332.
- [11] H. Yamaura, K. Moriya, N. Miura, N. Yamazoe, Mechanism of sensitivity promotion in CO sensor using indium oxide and cobalt oxide, *Sens. Actuators, B* 65 (2000) 39–41.
- [12] P. Thilakan, J. Kumar, Oxidation dependent crystallization behavior of IO and ITO thin films deposited by reactive thermal deposition technique, *Mater. Sci. Eng., B* 55 (1998) 195–200.
- [13] P. Thilakan, J. Kumar, Studies on the preferred orientation changes and its influenced properties on ITO thin films, *Vacuum* 48 (1997) 463–466.
- [14] M. Bender, N. Katsarakis, E. Gagaoudakis, E. Hourdakis, E. Douloufakis, V. Cimalla, G. Kiriakidis, Dependence of the photoreduction and oxidation behavior of indium oxide films on substrate temperature and film thickness, *J. Appl. Phys.* 90 (10) (2001) 5382–5387.
- [15] H. Fritzsche, B. Pashmakov, B. Clafin, Reversible changes of the optical and electrical properties of amorphous InO_x by photoreduction and oxidation, *Sol. Energy Mater. Sol. Cells* 32 (4) (1994) 383–393.
- [16] G. Kiriakidis, H. Ouacha, N. Katsarakis, K. Galatsis, W. Wlodarski, Low temperature InO_x thin films for O_3 and NO_2 gas sensing, *Proc. SPIE* 5116 (2003) 84–91.
- [17] H. Wohltjen, R. Dessy, Surface acoustic wave probe for chemical analysis. I. Introduction and instrument description, *Anal. Chem.* 51 (9) (1979) 1458–1475.
- [18] W.P. Jakubik, M.W. Urbanczyk, S. Kochowski, J. Bodzenta, Palladium and phthalocyanine bilayer films for hydrogen detection in a surface acoustic wave sensor system, *Sens. Actuators, B* 96 (2003) 321–328.
- [19] G. Kiriakidis, Nanostructured holographic recording utilizing InO_x photorefractive thin films, *Proc. SPIE* 5118 (2003) 117–124.
- [20] E. Gagaoudakis, M. Bender, E. Douloufakis, E. Natsakou, V. Cimalla, G. Kiriakidis, The influence of deposition parameters on room temperature ozone sensing properties of InO_x films, *Sens. Actuators, B* 80 (2001) 155–161.
- [21] M. Sucheá, G. Kiriakidis, Atomic force microscopy analysis of polycrystalline indium oxide thin films, in: *Poster Presented in XIX National Conference in Solid State and Material Science, Thessaloniki, Greece, September 21–24, 2003.*
- [22] M. Ivanovskaya, A. Gurlo, P. Bogdanov, Mechanism of O_3 and NO_2 detection and selectivity of In_2O_3 sensors, *Sens. Actuators, B* 77 (2001) 264–267.